Applied Physics Letters

Self-assembly of a lateral quasi-Ohmic $CuInSe_2$/InSe isotype heterojunction for flexible devices by pulsed laser deposition

Cite as: Appl. Phys. Lett. **115**, 162104 (2019); https://doi.org/10.1063/1.5123401
Submitted: 05 August 2019 . Accepted: 05 October 2019 . Published Online: 15 October 2019

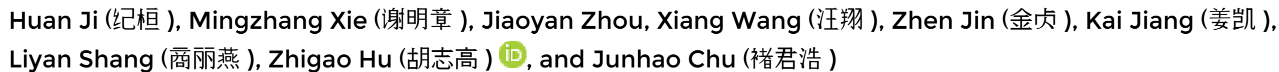

Huan Ji (纪桓), Mingzhang Xie (谢明章), Jiaoyan Zhou, Xiang Wang (汪翔), Zhen Jin (金贞), Kai Jiang (姜凯), Liyan Shang (商丽燕), Zhigao Hu (胡志高), and Junhao Chu (褚君浩)

View Online

Export Citation

CrossMark

Challenge us.
What are your needs for periodic signal detection?

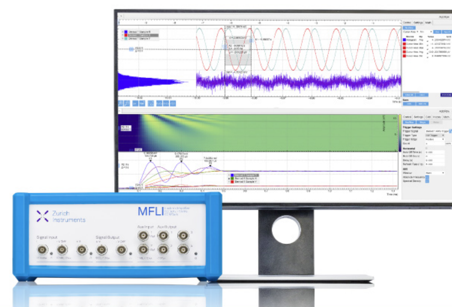

AIP Publishing

© 2019 Author(s).

Applied Physics Letters ARTICLE scitation.org/journal/apl

Self-assembly of a lateral quasi-Ohmic $CuInSe_2$/InSe isotype heterojunction for flexible devices by pulsed laser deposition

Cite as: Appl. Phys. Lett. **115**, 162104 (2019); doi: 10.1063/1.5123401
Submitted: 5 August 2019 · Accepted: 5 October 2019 ·
Published Online: 15 October 2019

View Online

Export Citation

CrossMark

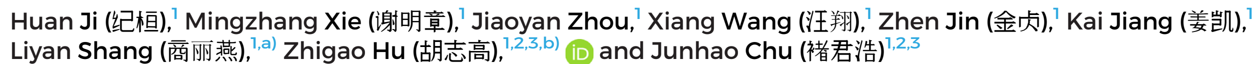
Huan Ji (纪桓),[1] Mingzhang Xie (谢明章),[1] Jiaoyan Zhou,[1] Xiang Wang (汪翔),[1] Zhen Jin (金贞),[1] Kai Jiang (姜凯),[1] Liyan Shang (商丽燕),[1,a)] Zhigao Hu (胡志高),[1,2,3,b)] and Junhao Chu (褚君浩)[1,2,3]

AFFILIATIONS

[1]Technical Center for Multifunctional Magneto-Optical Spectroscopy (Shanghai), Department of Materials, School of Physics and Electronic Science, East China Normal University, Shanghai 200241, China
[2]Collaborative Innovation Center of Extreme Optics, Shanxi University, Taiyuan, Shanxi 030006, China
[3]Shanghai Institute of Intelligent Electronics and Systems, Fudan University, Shanghai 200433, China

[a)]Electronic mail: lyshang@ee.ecnu.edu.cn
[b)]Electronic mail: zghu@ee.ecnu.edu.cn

ABSTRACT

The contacts between two-dimensional InSe films and metal electrodes play an important role in nanoelectronics flexible devices. Generally, there is a large work function difference between the Au and InSe films, which would form a Schottky contact to deteriorate device performances. Herein, we designed a lateral self-assembled $CuInSe_2$/InSe isotype heterojunction on a flexible mica substrate by pulsed laser deposition, which could improve the contact performances between electrodes and InSe films. By combining the X-ray photoelectron spectroscopy and Kelvin probe force microscopy results, the In rich $CuInSe_2$ and InSe regions could act as quasi-n^+-n junctions for reduction of the contact resistance with electrodes. Compared to the InSe films with Au electrodes, the $CuInSe_2$/InSe isotype heterojunction presents approximately half channel resistance and four times photocurrent values. Moreover, the heterojunction devices can still maintain relatively good performance under bending states by restraining the dark current. The present work proves the potential of $CuInSe_2$/InSe isotype heterojunctions for flexible applications.

Published under license by AIP Publishing. https://doi.org/10.1063/1.5123401

The discovery of graphene opened the fantastic field of two-dimensional (2D) layered semiconductors. Numerous works have been pursued urgently on 2D thin film materials, including graphene, transition metal dichalcogenides (TMDs), black phosphorus, III–VI binary chalcogenides, and so on.[1–5] As one of the III–VI binary chalcogenide layered material family, indium selenide (InSe) has attracted much interest for its promising properties in flexible photoelectricity, optical spectroscopy, thermal devices, novel devices, and so on.[5–8] Due to the strong quantum confinement effect (QCE), InSe possesses very interesting electronic band transition from a direct semiconductor to an indirect semiconductor as the layers are reduced to 5 nm. At the same time, its bandgap undergoes a large spread variation from 1.2 to 2.2 eV when reduced down to a monolayer.[1] The bandgaps of InSe cover a large spread range from visible to infrared. Its high photoresponse is very suitable for applications in photodetectors.[4,5,9] Like other 2D materials, InSe also possesses a unique advantage in applications of ultrahigh flexibility.[10]

As we know, previous studies mainly focused on the improvement of electrical performance[11,12] because InSe has light electron effective mass ($m^* = 0.143m_0$) and weak electron-phonon scattering.[13] Generally, the contacts between metal and semiconductors in nanoelectronics devices are very important in determining device performances. However, the contact between an InSe film and Au is a large Schottky contact (0.7 eV) under most conditions,[9] which performs as a barrier preventing the charge injection from the semiconductor to metal. Besides, the direct contacts between InSe films and Au are usually uniform. The electrodes are easy to falloff under large bending states, which can make devices fail. However, there are a few works focused on improving the contact performance between metals and InSe by heterojunctions. It is limited by the common fabricated approaches. The main approach to achieve high quality InSe nanosheets is from the mechanical exfoliation,[3] which is uncontrollable. Chemical vapor deposition (CVD) has poor repeatability, owing to the

active valence electrons of In atoms and many polytypes of different compounds In_xSe_y. It is hard to avoid oxygen during the process of crystallization in CVD.[7,14] As a typical bottom-up physical method, pulsed laser deposition (PLD) is widely used for achieving many high-quality oxide thin films and complex function materials.[15] Recently, PLD has been used in fabricating 2D materials due to its outstanding advantages, such as the quantitative stoichiometry, digital control of the film thickness, and high growth rate, which make it easy to maintain the consistency of synthesis conditions.[8,16] Thus, we fabricated the $CuInSe_2$/InSe heterojunction films by the PLD technique.

In this Letter, we designed a lateral $CuInSe_2$/InSe isotype heterojunction in one step. Due to the dopants in $CuInSe_2$ regions, the electronic band can be modulated to optimize the metal-semiconductor contacts. As a result, the quasi-Ohmic contact can greatly reduce the contact resistance. Then, $CuInSe_2$/InSe isotype heterojunction devices show more obvious photocurrent and large responsivity than pure InSe devices. Moreover, the $CuInSe_2$/InSe heterojunction presents promising potential for flexible applications because the large compressive strain can restrain its dark current.

First, Cu or Au electrodes of 50 nm thickness were patterned onto mica substrates by thermal evaporation. The channels between two electrodes are 50 μm long and 1200 μm wide. The substrate was heated to 400 °C and set 4.5 cm away from the InSe target (99.99%, 1 in. in diameter). The system pressure was maintained at 5.0×10^{-2} mbar by introducing highly pure argon. The KrF excimer pulsed laser ($\lambda = 248$ nm) output is obtained at 10 Hz. The total pulse number is 500 to maintain the same thickness of about 3 nm.

The structural characteristics were analyzed by X-ray diffraction (XRD, Bruker D8 Advance diffractometer, 1 cm spot diameter). The Raman scattering measurements were implemented using a Jobin-Yvon LabRAM HR Evolution spectrometer (532 nm laser, 3 μm spot diameter). The surface morphologies of $CuInSe_2$/InSe films were observed using a scanning electron microscope (SEM, PHILIPS XL30TMP system). X-ray photoelectron spectroscopy (XPS, RBD-upgraded PHI-5000C ESCA system, PerkinElmer, 10 μm spot diameter) with Mg Kα radiation ($h\nu = 1253.6$ eV) was carried out to analyze the valence states and stoichiometries of the films. The thickness and surface potential images of the films were obtained from the atomic force microscopy (AFM) and Kelvin probe force microscopy (KPFM) techniques (Bruker, Dimension Icon SPM), respectively. A Keithley 4200-SCS was used to measure the optoelectronic properties under the illumination of a 405 nm laser.

During the deposition, the energetic In and Se atoms can reassemble Cu atoms from the Cu electrodes. Finally, the $CuInSe_2$ regions formed within the lateral diffusion length of Cu, as shown in Fig. 1(a). The reaction can be expressed as follows: $2InSe + Cu \rightarrow CuInSe_2 + In$. The ratio of Cu to In can result in the change of $CuInSe_2$ electronical properties. XRD was used to clarify the crystallographic phase of both InSe and $CuInSe_2$. As shown in Fig. 1(b), the InSe peaks (10.6°, 21.2°, and 32.3°) could clearly agree with the standard database (JCPDS 34–1431).[8,11] It indicates the textured preferential orientation of the *c*-axis on mica substrates. In Fig. 1(c), the Raman spectra indicate the lattice vibration in InSe films. The peaks are located around 114.7 cm^{-1} (A_1'), 176.5 cm^{-1} (E''), 202.3 cm^{-1} (A_2''-LO), 212.5 cm^{-1} (E'-LO), and 227.1 cm^{-1} (A_1'), respectively. By combining the XRD and Raman spectra, InSe grown by the PLD method corresponds to the hexagonal crystal structure ε-phase (space group: D_{3h}). As shown in Fig. 1(b), the

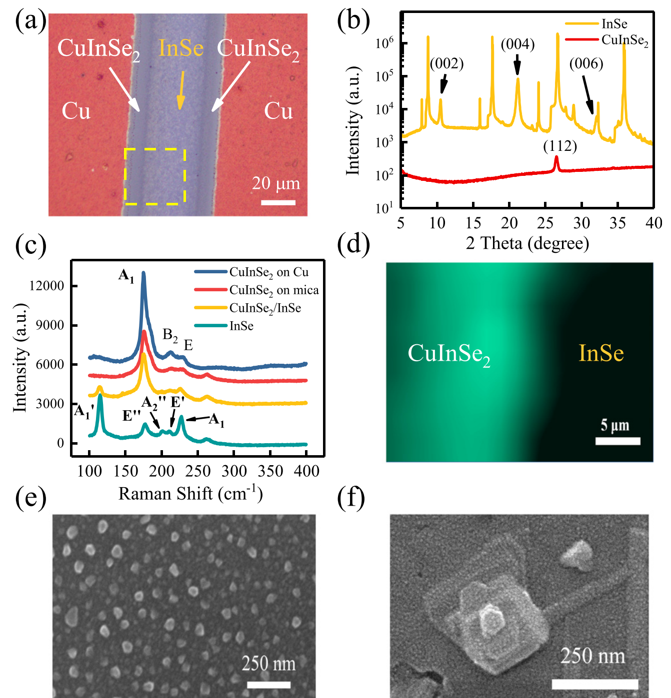

FIG. 1. (a) The optical image of a lateral $CuInSe_2$/InSe/$CuInSe_2$ heterojunction device. Raman mapping and KPFM were applied in the yellow broken line box. (b) XRD patterns of InSe and $CuInSe_2$ films, respectively. (c) Raman spectra of InSe and $CuInSe_2$ junctions, and the peak at 260 cm^{-1} belongs to mica substrates. (d) Raman mapping of $CuInSe_2$ (A_1, 174.8 cm^{-1}). The SEM images of (e) the $CuInSe_2$ region and (f) the InSe region, respectively.

XRD result for the $CuInSe_2$ film was measured on a copper-coated mica substrate. The pattern contains only one pronounced peak located at 26.6°, which can be indexed as (112) from the standard database (JCPDS 87–2265).[17] The Raman spectra of the $CuInSe_2$ regions were also obtained as shown in Fig. 1(c). It shows the peaks around 174.8 cm^{-1} (A_1), 212.0 cm^{-1} (B_2), and 229.5 cm^{-1} (E), respectively.[18] By combining the XRD and Raman results, it is found that $CuInSe_2$ is of the chalcopyrite structure (space group: $I\bar{4}2d$). Raman mapping was used to distinguish the boundary between $CuInSe_2$ and InSe regions by tracking the vibration peaks of $CuInSe_2$ (A_1, 174.8 cm^{-1}). As shown in Fig. 1(d), a clear boundary can be observed. The width of the $CuInSe_2$ regions is about 10 μm. The SEM images show a different surface morphology of two sides, as can be seen in Figs. 1(e) and 1(f). A sheetlike layered InSe morphology could be observed. However, layered InSe in the regions around Cu transformed into nonlayered $CuInSe_2$.

The detailed chemical composition of the heterojunction was analyzed by the XPS technique. Figure 2(a) shows the typical overall XPS spectra of InSe and $CuInSe_2$. As shown in Figs. 2(b) and 2(d), the In binding energy spectra of both InSe and $CuInSe_2$ can be fitted into In $3d_{3/2}$ and In $3d_{5/2}$, respectively, with the 7.6 eV split from a spin–orbit interaction. The results correspond to In^{3+}.[14,19,20] As shown in Figs. 2(c) and 2(e), the Se spectra of both InSe and $CuInSe_2$ can be fitted into Se $3d_{3/2}$ and Se $3d_{5/2}$, respectively, with the separation of 0.9 eV. The results correspond to Se^{2-}.[9,14,19] However, InSe consists of two Se^{2-} anions and a $[In_2]^{4+}$ diatomic cation.[20] As shown in Fig. 2(f),

Published under license by AIP Publishing

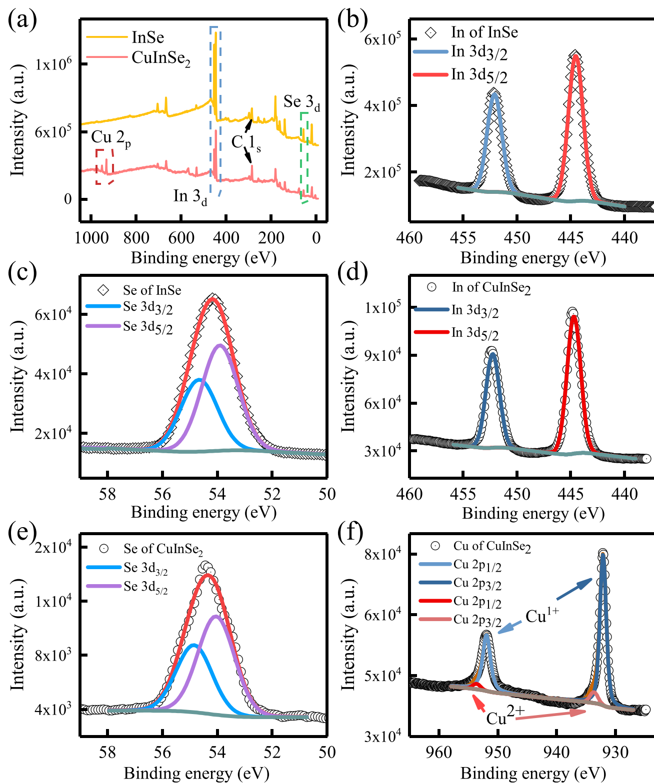

FIG. 2. (a) The overall XPS spectra of InSe and $CuInSe_2$. The fitted XPS spectra of (b) In 3d and (c) Se 3d in InSe films. The fitted XPS spectra of $CuInSe_2$ (d) In 3d, (e) Se 3d, and (f) Cu 2p, respectively.

there are two Cu 2p species with different spin–orbit splittings in the Cu spectrum. The peaks are located at Cu $2p_{1/2}$ (951.9 eV) and Cu $2p_{3/2}$ (932.0 eV), which correspond to Cu^{+}. On the other hand, the peaks are located at Cu $2p_{1/2}$ (953.4 eV) and Cu $2p_{3/2}$ (933.2 eV), which act as the shoulder peaks and correspond to Cu^{2+}.[19,21–23] The intensity of the Cu^{2+} shoulder peaks indicates that the ratio of Cu^{2+} is much less than that of Cu^{+}. The stoichiometric ratio of In:Se was calculated to be 1.08:1, which is much close to the theoretical value of single phase InSe. The ratio of Cu:In:Se is about 0.6:1.0:1.3. Because the ratio of Cu to In affects the electrical performance of $CuInSe_2$, the Cu-poor and In-rich chemical composition would lead the $CuInSe_2$ regions to work as n-type semiconductors.[24,25]

We utilized KPFM to further verify the charge transfer mechanism and electronic band structure evolution in the $CuInSe_2$/InSe heterojunction. It could provide the intrinsic Fermi levels, surface electric field, and widths of space charge regions in the thermal equilibrium $CuInSe_2$/InSe heterojunction. The contact potential difference (CPD) between the tip and the local area of InSe or $CuInSe_2$ can be expressed as

$$\begin{aligned} CPD_{\mathrm{InSe}} &= W_{\mathrm{tip}} - W_{\mathrm{InSe}}, \\ CPD_{\mathrm{CuInSe_2}} &= W_{\mathrm{tips}} - W_{\mathrm{CuInSe_2}}, \end{aligned} \tag{1}$$

where W_{tip}, W_{InSe}, and W_{CuInSe_2} are the surface work function of the AFM tip, InSe, and $CuInSe_2$, respectively.[26] Figure 3(a) shows the clear surface potential image from the edge of $CuInSe_2$ to the channel center of the InSe region. There are two distinct regions of the $CuInSe_2$/InSe lateral isotype heterojunction. The distinction between the Fermi levels of $CuInSe_2$ and InSe can be easily calculated by estimating $\Delta CPD_{\mathrm{CuInSe_2-InSe}}$, as shown in Fig. 3(b). It can be given as

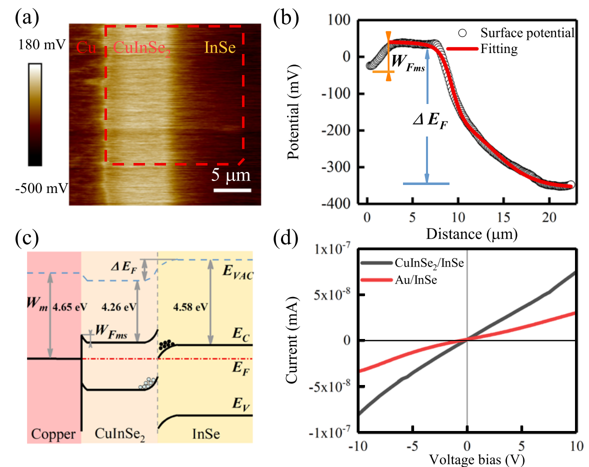

FIG. 3. (a) The KPFM image of the lateral device. The average surface potential is shown in a red broken line box. (b) The surface potential and the fitting of the $CuInSe_2$/InSe heterojunction. (c) The energy band distribution of the $CuInSe_2$/InSe heterojunction with the Cu electrode. (d) The current vs bias voltage characteristic in the dark.

$$\begin{aligned} \Delta E_F &= E_{F_{\mathrm{CuInSe_2}}} - E_{F_{\mathrm{InSe}}} = e(CPD_{\mathrm{CuInSe_2}} - CPD_{\mathrm{InSe}}) \\ &= e\Delta CPD = e(W_{\mathrm{InSe}} - W_{\mathrm{CuInSe_2}}). \end{aligned} \tag{2}$$

The difference from Fermi levels is $\Delta E_F \approx 0.35$ eV. The depletion width is approximately 12 μm, indicating a graded junction.[29] The distribution of the surface potential can be well fitted by a BiDoseResp function. From the differential of the fitting function, the approximate distribution of the electric field could be derived. The maximum electric field $\xi_m(x_0)$ is 0.9 mV/μm. x_0 is 9.6 μm, which is the location of the frontier between the two regions. It is much close to the Raman mapping results.

The energy bandgap of InSe is given as 1.5 eV and that of $CuInSe_2$ is 1.0 eV, respectively.[9,30,31] The electron affinity for InSe and $CuInSe_2$ is 4.58 eV and 4.26 eV.[27,28] As shown in Fig. 3(c), the Fermi level of $CuInSe_2$ is about 0.35 eV higher than that of InSe, which means that electrons in the $CuInSe_2$ side fill higher energy levels than that in the InSe side. Then, those electrons transfer from the $CuInSe_2$ side to the InSe side through the interface. Thus, charges can be accumulated in the InSe side, which results in the downward energy band. In contrast, holes can be accumulated in the $CuInSe_2$ side, which results in the upward energy band. Then, the electric field is observed from the $CuInSe_2$ side to the InSe side. After the drift current caused by the built-in electrical field could counterbalance the diffusion current, the heterojunction attains thermal equilibrium. The electric field would accelerate electrons toward the InSe channel, which could decrease channel resistance. This lateral heterojunction can work as a quasi-n^{+}-n junction, where InSe is the quasi-n-side and $CuInSe_2$ is the quasi-n^{+}-type, respectively.[32,33] The built-in electrical field results in

Published under license by AIP Publishing

the separation of charges and holes within this long depletion, when external light is cast upon the heterojunction devices. Then, charges and holes flow in opposite directions. This built-in electrical field could improve the photoelectric effect, which is better than pure InSe channels. The potential drop at the $CuInSe_2$ and Cu electrode interface is very little ($W_{F_{ms}} \approx 0.05$ eV), which is a very small voltage of the Schottky barrier, as shown in Fig. 3(b). It is much less than the large work function difference of 0.7 eV between Au and InSe films.[9] As shown in Fig. 3(d), the linearity I-V curve of $CuInSe_2$/InSe heterojunctions indicates the quasi-Ohmic contact between electrodes and films. With the increase in voltage bias from −10 V to 10 V, the channel current increases almost linearly. However, the Au electrode devices have a large channel resistance, which is about 2.4 times that of the heterojunction. Compared with $CuInSe_2$ regions, the InSe region is a high resistance region. Unlike the 50 μm long pure InSe channel in the Au/InSe device, the channel in the heterojunction device consists of 20 μm long $CuInSe_2$ and 30 μm long InSe. Moreover, the in-built electrical field between InSe and $CuInSe_2$ regions can further reduce the resistance in the heterojunction. The large work function difference between Au and InSe films is another factor, which also results in the poor linearity of the Au device curve. The barrier would obstruct electron motion from films to electrodes. The two Schottky barriers, between two Au electrodes and the channel film, respectively, show a difference, which leads the curve of the Au device to deviate from the origin of axes.

Because of the photoelectric response in $CuInSe_2$ regions, the photosensitive area in the heterojunction device is the same as that in the pure InSe device. Figure 4(a) presents the photocurrent ($I_{ph} = I_{light} - I_{dark}$) of the $CuInSe_2$/InSe isotype heterojunction and pure InSe devices. Responsivity (R) is defined as $R = I_{ph}/PS$, where P is the light power density and S is the effective photosensitive area. At the same laser (405 nm, 3 mm spot diameter) intensity of 1.16 mW/cm^2 and a bias voltage of 10 V, the R value of the Au electrode device is 0.036 mA/W. The R value of the heterojunction is 0.147 mA/W, which is increased to 4 times of the former. Figure 4(b) shows the photoswitching curves of the heterojunction device at different illumination powers. With the increase in incident light power, the device shows more obvious I_{ph}. The on/off ratio increases to almost 40 under the light intensity of 31.3 mW/cm^2. The rising and decay response times of the heterojunction are measured to be 0.3 s and 0.6 s, respectively, which are superior to those of many other 2D photodetectors.[9,34]

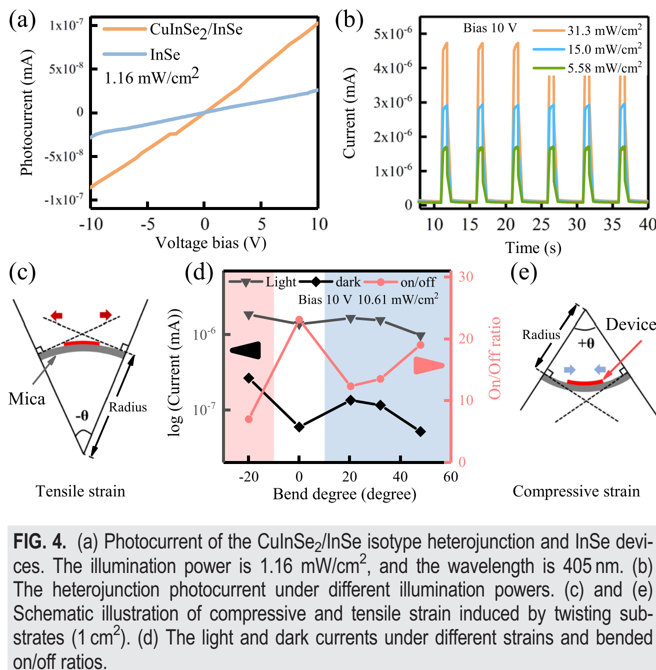

FIG. 4. (a) Photocurrent of the $CuInSe_2$/InSe isotype heterojunction and InSe devices. The illumination power is 1.16 mW/cm^2, and the wavelength is 405 nm. (b) The heterojunction photocurrent under different illumination powers. (c) and (e) Schematic illustration of compressive and tensile strain induced by twisting substrates (1 cm^2). (d) The light and dark currents under different strains and bended on/off ratios.

We have further explored the heterojunction properties under the flexible condition. As shown in Figs. 4(c) and 4(e), the larger bent state corresponds to the smaller radius of curvature (θ). Under the tensile strain, the radius of 20° is 2.865 cm. While under the compressive strain, the radii of 20°, 32°, and 48° are 2.865 cm, 1.790 cm, and 1.194 cm, respectively. Zero degree means no external strain. The heterojunction device was consistently illuminated under the same laser power (15.0 mW/cm^2, 405 nm), and the voltage bias was 10 V. As shown in Fig. 4(d), the dark current changed more obviously than the light current under the external strain. With the increasing compressive strain, the dark light was restrained gradually. Thus, the on/off ratio can be increased under a large bent degree.

In conclusion, we have designed a lateral self-assembled $CuInSe_2$/InSe isotype heterojunction and fabricated by the PLD technique. The $CuInSe_2$/InSe lateral isotype heterojunction could act as an n^+-n junction. It could improve the contact performance between InSe films and electrodes. Further, we systematically compared the performance of both pure InSe and $CuInSe_2$/InSe isotype heterojunction devices. The $CuInSe_2$/InSe isotype heterojunction devices showed quasi-Ohmic linearity and larger channel current. The photocurrent of the heterojunction increased to about 4 times higher than that of the pure InSe device. It also confirms that a large compressive strain could restrain the dark current and lead to the increasing on/off ratio. The $CuInSe_2$/InSe heterojunction proves the potential for flexible applications.

This work was financially supported by the National Key R&D Program of China (Grant Nos. 2017YFA0303403 and 2018YFB0406500), the Natural Science Foundation of China (Grant Nos. 61674057 and 91833303), the Projects of Science and Technology Commission of Shanghai Municipality (Grant Nos. 18JC1412400, 18YF1407200, and 18YF1407000), and the Program for Professor of Special Appointment (Eastern Scholar) at Shanghai Institutions of Higher Learning.

REFERENCES

[1] G. W. Mudd, S. A. Svatek, T. Ren, A. Patanè, O. Makarovsky, L. Eaves, P. H. Beton, Z. D. Kovalyuk, G. V. Lashkarev, Z. R. Kudrynskyi, and A. I. Dmitriev, Adv. Mater. **25**, 5714 (2013).
[2] K. L. Li, Y. H. Hong, Z. W. Li, and X. K. Liu, Appl. Phys. Lett. **113**, 021903 (2018).
[3] D. A. Bandurin, A. V. Tyurnina, G. L. Yu, A. Mishchenko, V. Zólyomi, S. V. Morozov, R. K. Kumar, R. V. Gorbachev, Z. R. Kudrynskyi, S. Pezzini, Z. D. Kovalyuk, U. Zeitler, K. S. Novoselov, A. Patanè, L. Eaves, I. V. Grigorieva, V. I. Falko, A. K. Geim, and Y. Cao, Nat. Nanotechnol. **12**, 223 (2017).
[4] H. W. Yang, H. F. Hsieh, R. S. Chen, C. W. Ho, K. Y. Lee, and L. C. Chao, ACS Appl. Mater. Interfaces **10**, 5740 (2018).
[5] S. R. Tamalampudi, Y. Y. Lu, U. R. Kumar, R. Sankar, C. D. Liao, B. K. Moorthy, C. H. Cheng, F. C. Chou, and Y. T. Chen, Nano Lett. **14**, 2800 (2014).

Published under license by AIP Publishing

[6]H. W. Hu, Y. L. Sun, M. S. Chai, D. Xie, J. Ma, and H. W. Zhu, Appl. Phys. Lett. **114**, 252903 (2019).
[7]W. J. Huang, L. Gan, H. Q. Li, Y. Ma, and T. Y. Zhai, Chem. Eur. J. **24**, 15678 (2018).
[8]D. H. Zheng, J. Shiogai, K. Fujiwara, and A. Tsukazaki, Appl. Phys. Lett. **113**, 253501 (2018).
[9]Z. B. Yang, W. J. Jie, C. H. Mak, S. H. Lin, H. H. Lin, X. F. Yang, F. Yan, S. P. Lau, and J. H. Hao, ACS Nano **11**, 4225 (2017).
[10]Y. Li, T. M. Wang, M. Wu, T. Cao, Y. W. Chen, R. Sankar, R. Ulaganathan, F. C. Chou, C. Wetzel, C. Y. Xu, S. G. Louie, and S. F. Shi, 2D Mater. **5**, 021002 (2018).
[11]W. Feng, W. Zheng, W. W. Cao, and P. A. Hu, Adv. Mater. **26**, 6587 (2014).
[12]M. J. Li, C. Y. Lin, S. H. Yang, Y. M. Chang, J. K. Chang, F. S. Yang, C. R. Zhong, W. B. Jian, C. H. Lien, C. H. Ho, H. J. Liu, R. Huang, W. W. Li, Y. F. Lin, and J. H. Chu, Adv. Mater. **30**, 1803690 (2018).
[13]S. Sucharitakul, N. J. Goble, U. R. Kumar, R. Sankar, Z. A. Bogorad, F. C. Chou, Y. T. Chen, and X. P. A. Gao, Nano Lett. **15**, 3815 (2015).
[14]H. C. Chang, C. L. Tu, K. I. Lin, J. Pu, T. Takenobu, C. N. Hsiao, and C. H. Chen, Small **14**, 1802351 (2018).
[15]J. Y. Zhou, M. Z. Xie, A. Y. Cui, B. Zhou, K. Jiang, L. Y. Shang, Z. G. Hu, and J. H. Chu, ACS Appl. Mater. Interfaces **10**, 30548 (2018).
[16]Z. B. Yang and J. H. Hao, J. Mater. Chem. C **4**, 8859 (2016).
[17]Z. Q. Zheng, J. D. Yao, and G. W. Yang, ACS Appl. Mater. Interfaces **9**, 7288 (2017).
[18]W. Feng, W. Zheng, X. S. Chen, G. B. Liu, W. W. Cao, and P. A. Hu, Chem. Mater. **28**, 983 (2015).
[19]J. J. Wang, Y. Q. Wang, F. F. Cao, Y. G. Guo, and L. J. Wan, J. Am. Chem. Soc. **132**, 12218 (2010).
[20]J. Lauth, F. E. S. Gorris, M. S. Khoshkhoo, T. Chasse, W. Friedrich, V. Lebedeva, A. Meyer, C. Klinke, A. Kornowski, M. Scheele, and H. Weller, Chem. Mater. **28**, 1728 (2016).
[21]A. Olvera, P. Sahoo, S. Tarczynski, and P. F. P. Poudeu, Chem. Mater. **27**, 7179 (2015).
[22]Y. N. Liang, K. Yu, Q. Yan, and X. Hu, ACS Appl. Mater. Interfaces **5**, 4100 (2013).
[23]S. Kim, M. Kang, S. Kim, J. H. Heo, J. H. Noh, S. H. Im, S. I. Seok, and S. W. Kim, ACS Nano **7**, 4756 (2013).
[24]N. B. Chaure, J. Young, A. P. Samantilleke, and I. M. Dharmadasa, Sol. Energy Mater. Sol. Cells **81**, 125 (2004).
[25]C. Persson, Y. Zhao, S. Lany, and A. Zunger, Phys. Rev. B **72**, 035211 (2005).
[26]T. Jiang, F. Wang, A. Y. Cui, S. Guo, K. Jiang, L. Y. Shang, Z. G. Hu, and J. H. Chu, Nanotechnology **29**, 435703 (2018).
[27]M. K. L. Man, A. Margiolakis, S. D. Jones, T. Harada, E. L. Wong, M. B. M. Krishna, J. Madeo, A. Winchester, S. Lei, R. Vajtai, P. M. Ajayan, and K. M. Dani, Nat. Nanotechnol. **12**, 36 (2017).
[28]T. Maeda, W. Gong, and T. Wada, Jpn. J. Appl. Phys., Part 1 **55**, 04ES15 (2016).
[29]W. Melitz, J. Shen, A. C. Kummel, and S. Lee, Surf. Sci. Rep. **66**, 1 (2011).
[30]S. M. Chauhan, S. H. Chaki, M. P. Deshpande, J. P. Tailor, A. J. Khimani, and A. V. Mangrola, Nano-Struct. Nano-Objects **16**, 200 (2018).
[31]A. B. Rohom, P. U. Londhe, and N. B. Chaure, J. Electrochem. Soc. **165**, H3051 (2018).
[32]K. Chen, X. Wan, W. G. Xie, J. X. Wen, Z. W. Kang, X. L. Zeng, H. J. Chen, and J. B. Xu, Adv. Mater. **27**, 6431 (2015).
[33]Z. J. Pan, W. B. Peng, F. P. Li, and Y. N. He, Adv. Funct. Mater. **28**, 1706897 (2018).
[34]L. Jiao, W. J. Jie, Z. B. Yang, Y. H. Wang, Z. W. Chen, X. Zhang, W. H. Tang, Z. P. Wu, and J. H. Hao, J. Mater. Chem. C **7**, 2522 (2019).

Published under license by AIP Publishing